Interaction between connectivity and oscillatory currents in a heterogeneous neuronal network

Troy Lau and Michal Zochowski

Phys. Rev. E **83**, 051908 — Published 11 May 2011

DOI: 10.1103/PhysRevE.83.051908

Interaction between connectivity and oscillatory currents in a heterogeneous neuronal network

Troy Lau[1] and Michal Zochowski[1,2]

[1]*Department of Physics, University of Michigan, Ann Arbor, MI, 48109*

[2]*Biophysics Program, University of Michigan, Ann Arbor, MI, 48109*

Abstract

Intrinsic oscillations are thought to play important and distinct roles in cognitive processes across nearly all regions of the brain. Their specific roles are highly dependent on their properties: low frequency theta is thought to be important in the gating of cognitive processes while high frequency gamma is believed to be essential for binding and spike timing dependent plasticity. We investigated the role of an oscillatory drive for pattern formation of heterogeneous networks. Network heterogeneities were implemented as network regions having increased connectivity as compared to the rest of the network. We varied the properties of the oscillatory drive as well as network connectivity. We observed that the disparity in spatio-temporal patterning of activity between the structurally enhanced region and rest of the network was highly dependent on frequency and amplitude of the oscillatory drive as well as network connectivity, generally favoring bigger enhancement of activity for high frequency oscillations and phase locking with moderate enhancement of activity for lower frequency oscillations. Thus, these results indicate that the specific role of the observed oscillations may depend on their dynamical interactions with the heterogeneous network.

I. INTRODUCTION

The oscillatory patterning of neural activity is ubiquitous and is thought to play a major role, in many functions, across nearly all regions of the brain [1–10]. Delta (1-4 Hz) [11], theta (4-10 Hz)[4, 12], alpha (8-12 Hz)[11], and gamma (25-100 Hz)[2, 3, 13–16] frequencies are more than just categorical denominations as each range is prominent and have independent functions in different areas. Accordingly, a considerable amount of work has been dedicated to the mechanisms involved in the generation of these oscillations (for example [15, 17, 18] and references therein). These mechanisms can be broadly divided into two groups: intrinsic cellular mechanisms and network based mechanisms. It is known that single cells can exhibit intrinsic oscillatory rhythms that are mediated by sub-threshold voltage dependent currents or after hyperpolarization [15, 18–21]. For example, fast-spiking interneurons are postulated to be responsible for the the generation of high-frequency gamma rhythms through fast repolarization and gap-junction synchronization inducing global inhibition [22, 23]. From a network perspective, studies have shown that interacting cell assemblies can also mediate the formation of oscillatory patterning of their activity [15, 17, 24]. Recent work by Vervaeke et al. has demonstrated a (de)synchronization dependence on the local organization of the chemical synaptic connections in the Golgi interneuron network of the cerebellum [25].

An equally extensive amount of research has focused on the role of these oscillations during information processing. Various studies have demonstrated their role during learning [4], various stages of sleep [26], and recall [4] amongst many other processes. Oscillations are thought to act as a gating mechanism [27, 28], aid in binding via spike-timing dependent plasticity [14], or serve in the coordination of large separated groups of neurons [29]. From a more physical perspective, input frequencies have also been studied in the context of stochastic resonance, or the enhancement of an oscillatory signal in the presence of specific noise [30–33].

Most of the work done until now has focused on the role of oscillations in homogeneous networks, i.e. networks having uniform structural and dynamical properties throughout their assembly [34, 35]. Brain networks however, are highly heterogeneous. Even within the same brain structures, such as the neocortex or hippocampus, the local network connectivity is being constantly altered by different processes. The long-term potentiation or depression of synapses that underlie learning lead to the selective formation of cells ensembles with higher

connectivity densities and increased synaptic connection strengths [36, 37]. Elucidation of dynamical pattering in heterogenous networks may lead to better understanding of dynamics of information storage end retrieval.

At the same time pathologic processes (e.g. brain injury or genetic malformations), such as the ones leading to epilepsy, may create local foci that later generate epileptic seizures. Understanding interaction of these foci with the intact networks may lead to easier identification of these pathological brain structures.

In this paper we focus on understanding how an oscillatory drive differentially interacts with structural heterogeneities in a neuronal network and how it may provide a dynamical backbone for information processing. Such an oscillatory drive may be generated both externally, as by the pacemaker medial septum leading the hippocampus [38], or from intrinsic sources, as by the slow-pyramidal and fast-basket cell interaction in the cortex [39]. We have found that the frequency of the input oscillation can act as a control parameter for the patterning of activity in the network. We show that for certain, large sets of network parameters, as well as specific ranges of frequency/amplitude of oscillation, the activity of the network region with modified structural properties can be selectively enhanced, resembling a network mediated resonance response. This enhancement is in the form of an increase in firing rate or in the increase of phase coherence of neuron spike times. Furthermore, the frequency ranges where the phase coherence of the heterogeneity are enhanced are significantly different than the frequency ranges where the firing rates are increased. These effects are modulated by the number of connections, synaptic coupling strength, and network structure.

Our results shed light on the interaction of structural network properties with oscillatory drives and provide an insight into the possible additional dynamical underpinnings of the differential roles of oscillatory drive in the neural networks. We demonstrate that otherwise similar input oscillations can have drastically different effects depending on the properties of the network structure, and therefore different functional roles in the brain.

II. MODELING

A. Network architecture

We modeled a neuronal network consisting of groups of 200 excitatory and 200 inhibitory neurons. Both groups were arranged on a 1-D lattice with periodic boundary conditions forming a ring structure. The network elements were coupled using the Small-World paradigm [40] where neurons are initially connected to their nearest neighbors within a radius r, then randomly rewired anywhere within the network with probability p. Thus, $p = 0$ returns a uniform and locally coupled network and $p = 1$ returns a randomly and globally coupled network. A more realistic proportion of excitatory to inhibitory neurons is 80% - 20% and we have used the 50% - 50% ratio for simplicity purposes only. The results of this paper are maintained for either ratio and we refer the reader to section III B 2 where we investigate a range of excitatory-inhibitory ratios. We used 1-D network model with periodic boundary conditions. Previous work has also shown the neuronal dynamics are readily translatable from 1-2-3D cases [41–43]. To insure the robustness of our results however we briefly investigate a 2-D network in Section III B 3.

There were four connection topologies to consider for these two networks: the connections within the excitatory network (r_e, p_e), within the inhibitory network (r_i, p_i), from the excitatory to the inhibitory network (r_{e-i}, p_{e-i}), and from the inhibitory network to the excitatory network (r_{i-e} , p_{i-e}). The connectivity radius of connection types were set to be the same, $r_e = r_i = r_{e-i} = r_{i-e} = r$. We varied the connectivity structure emanating from the excitatory network (rewiring parameter $p_e = p_{e-i} = p$) and investigated rewiring parameter values $p \in [0, 1]$. We set the connectivity emanating from inhibitory cells to be random $p_i = p_{i-e} = 1$.

B. Integrate-and-Fire neuron model

It is known that neurons, and accordingly oscillator neuron models, can have distinct and complex interactions with oscillatory depolarizing currents. The goal of this work was to understand the interactions that result from the network itself and not on effects stemming from the dynamics of single neurons. Therefore we have used the leaky integrate-and-fire neuron model throughout most of our simulations. This model lacks a oscillating properties

and a classical resonance frequency, therefore all frequency responses are direct properties of the network interactions themselves. This is not to say however, that the interaction between neuronal and network dynamics are not prevalent in real brain systems, quite the contrary is true, only that we seek to reduce the system to a network response to better understand this particular underlying mechanism. We briefly cover the the interactions with more complex resonating neuron models.

$$C\frac{dV^j}{dt} = -\alpha_j(V - V^j_{rest}) + I_{ext} + \sum_k w^k_{syn} S^{jk} I^k_{syn} \tag{1}$$

Here, V^j is the membrane potential of the j^{th} neuron, α is a leakage coefficient which is different for every cell, $1/R_s = \alpha_j \in [0, 0.1]\mu S$; I^k_{syn} is the synaptic current generated at the time of the spike, w^j_{syn} defines the excitatory or inhibitory synaptic coupling strength and each element positive/negative for excitatory/inhibitory neurons; S^{jk} is the synaptic connectivity (adjacency) matrix; and I_{ext} is an external current (see next section). We investigated a range of synaptic couplings $w_{syn} \in [0, 0.3]$ increments of 0.1. For the simulations in this paper the value of capacitance was $C = 0.5nF$ hence $\langle \tau_j \rangle = 10ms$ and $V_{rest} = -70mV$. We employed Euler's method to solve for the voltage with timesteps of $dt = 0.25ms$.

The synaptic current is activated after the presynaptic neuron reaches a threshold $V_{thresh} = -54mV$ and fires an action potential. The pre-synaptic neuron is then returned to V_{rest} and remains there for a refractory period $t_{ref} = 10ms$. The synaptic current is of the form:

$$I^k_{syn}(t) = (e^{\frac{-(t-t^k_{spike})}{\tau_s}} - e^{\frac{-(t-t^k_{spike})}{\tau_f}})I_{base} \tag{2}$$

where $I_{base} = 8nA$ scales the synaptic current, $(t - t^k_{spike})$ is the time since the last firing of the presynaptic neuron, $\tau_s = 3ms$ is the slow time constant, and $\tau_f = 0.3ms$ is the fast time constant. The variables τ_s and τ_f are chosen such that the post-synaptic potential lasts approximately 2 ms. There was a 2.5 ms synaptic delay between each neuron. We have investigated networks with different transmission delays and no major differences were detected.

To create the heterogeneity in the network, we selected a group of 20 adjacent neurons (usually IDs 90-110) and increased their synaptic coupling strength (w_{syn}) by 30% as compared to the rest of the network. This 30% increase was maintained when the overall w_{syn}

was increased for the entire network, unless otherwise stated. We referred to this region as the structurally enhanced region. Varying the size of this region did not have a qualitative effect on our results.

Additionally, each neuron was individually exposed to a Poisson noise. The noise probability was set to 0.05% per time step, resulting in an average firing rate of 2 Hz in the absence of any other input.

C. External oscillatory current

We controlled the oscillatory input into the network via the external current I_{ext}. Both the excitatory and inhibitory neurons were driven by the external oscillating current $\langle I_{ext} \rangle = 0$:

$$I_{ext} = A_{oss} sin(f_{dr} t + \delta), \tag{3}$$

where A_{oss} is the amplitude of the oscillation, f_{dr} is the driving frequency and δ is a random starting phase. We investigated $f_{dr} \in [3, 90] Hz$ in increments of 3 Hz and $A_{dr} \in [0.4, 1.2] nA$ in increments of 0.1 nA. This oscillation may be thought of as an external current source [38] or an intrinsically generated current source input into this specific population of neurons [25].

D. Resonate and fire neuron model

To better understand the generality of our results, we investigated the basic phenomena for two other classes of neurons: the resonate-and-fire and Hodgkin-Huxley Type I models. The resonate-and-fire neuron was based off the model presented by Izhikevich [44]. We selected the model because the classical resonance frequency/condition was easily modified and achieved. The model is a 2-D linear system where x is the current like internal variable and y is the voltage like internal variable. Here

$$\frac{dx}{dt} = -x - \omega y + I_{ext} + w_{syn,j} \sum_k S^{jk} I^k_{syn} \tag{4}$$

and

$$\frac{dy}{dt} = -\omega x - y \tag{5}$$

For a full discussion refer to [44]. For our analysis, we adjusted the parameters of the neuron, $\omega = 0.2, 0.3$, and 0.4 (all other values remain the same), to resonate at roughly 30, 45, and 60 Hz respectively.

E. Hodgkin Huxley neuron model

We selected a Type-I non-resonating Hodgkin Huxley interneuron neuron model based off Wang and Busaki [18] and generalized by Pfeuty et al. [45]. These neurons had two compartments (somatic and dendritic) with sodium, potassium, and leak currents, along with an excitatory and inhibitory coupling in the same manner as our simulations. A brief summary is provided below; for the detailed description we refer you to [18, 45]. The model is divided into a somatic compartment (s) and dendritic compartment (d). The dynamics of the somatic compartment are given by:

$$C\frac{dV^s}{dt} = -I_L - I_{Ns} - I_{Kdr} - g_c(V^s - V^d) + I_{noise}, \tag{6}$$

the dendritic compartment is described by:

$$C\frac{dV^d}{dt} = -I_{L,d} - g_c(V^d - V^s) + I_{ext}, \tag{7}$$

where the currents are $I_L = g_L(V^s - V_L)$, $I_{L,d} = g_L(V^d - V_L)$, $I_{Na} = g_{Na}m_\infty^3 h(V^s - V_{Na})$, and $I_K = g_K n^4(V^s - V_K)$.

I_L is the leak current, I_{Na} transient sodium current and I_{Kdr} is the delayed rectifier potassium current, m, h, n are voltage dependent conductances. We implemented these equations with following parameters: $g_{Na} = 35mS/cm^2, V_{Na} = 55mV, g_K = 9mS/cm^2, V_k = -75mV, g_L = 0.1mS/cm^2, g_c = 0.3mS/cm^2, V_L = -65mV, C = 1F/cm^2$

F. Analysis

We used two metrics to quantify the behavior of the network: regional firing rates (activity) and the mean phase coherence (MPC). The firing rate was defined as the number of firings per neuron per second and was calculated separately over the enhanced region and the rest of the network. To quantify how active the enhanced region was over the rest of

the network, we defined the activity ratio as the firing rate of the enhanced region divided by the firing rate of the rest of the network.

We used the MPC to measure the amount of phase locking between cells [44, 46]. The MPC ranges between 0 (least coherent) and 1 (most coherent). The MPC is calculated pairwise between neurons inter-spike-intervals via the equation, for the MPC (denoted below as $\mathcal{M}$) between neuron n and m:

$$\mathcal{M}_{nm} = \left| \frac{1}{S} \sum_{s=1}^{S} e^{i\phi_{nm_s}(j)} \right| \tag{8}$$

Here S is the total number of measurements of cell m-s spike times within the first and last firing of cell n and ϕ_{nm_s} is the phase between cell n and m for interval j containing s. The phase is defined as

$$\phi_{nm_s}(j) = 2\pi \frac{\tau_{n_j,m_s}}{\tau_{n_j}}, \tag{9}$$

where

$$\tau_{n_j} = t_{n_{j+1}} - t_{n_j}; \tag{10}$$

is the inter-spike-interval j for neuron n containing s and

$$\tau_{n_j,m_s} = t_{m_s} - t_{n_j}; \tag{11}$$

is the time difference between the initial firing of neuron n, on interval j, and the firing s, of neuron m, with the condition,

$$t_{n_j} \leq t_{m_s} \leq t_{n_{j+1}} \tag{12}$$

Finally, to calculate total MPC ($\mathcal{M}$) we take the average of all $\mathcal{M}_{nm}$ pairs across all neurons,

$$\mathcal{M} = \frac{1}{N(N-1)} \sum_{n}^{N} \sum_{m}^{N} \mathcal{M}_{nm} \tag{13}$$

where N is number of neurons in a group over which the mean phase coherence was calculated. We calculated MPC separately for the neural pairs composing the enhanced region and these in the rest of the network.

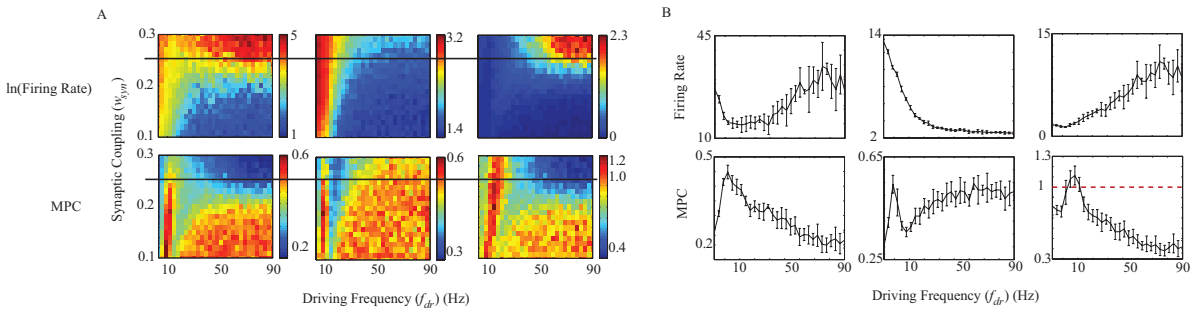

FIG. 1. Comparison of activity patterns between the structurally enhanced region and rest of the network. A) Top - The natural log of the firing rates for the enhanced region (left), rest of the network (center), and the natural log of ratio of the two (right). Bottom - the mean phase coherence for the corresponding regions. We varied the synaptic coupling and oscillation frequency while keeping the oscillation amplitude $A_{dr} = 0.8nA$ and connection radius $r = 3$ fixed. B) The same measures as before but for a specific value of synaptic coupling $w_{syn} = 0.25$. Parameter values correspond to the line drawn through the figure on the left.

G. Power spectral density

To compute the power spectral density (PSD) plots, we binned the total spiking output (10 ms bins) of the enhanced and outside region. This was simply a sum of ones (if the neuron fired) and zeros (if it did not). We then used the MATLAB Fast-Fourier Transform function on the complete 2000 ms simulation.

III. RESULTS

Our goal was to understand the interaction between network topology and oscillatory input on the dynamics of a heterogeneous neuronal network. For this reason we have created a network that has a localized region of increased connectivity (w_{syn} is fixed to 30% higher than the rest of the network). To investigate the differences of network response within the synaptically enhanced region, we measured the spiking activity and MPC within the region and within the rest of the network, and took the ratio of the two values. Throughout this paper we monitored these values as a function of the driving frequency f_{dr} of input.

We first studied the change of activity for the enhanced region, the outside region, and the ratio of these two while changing the oscillatory input frequency f_{dr} and the network coupling

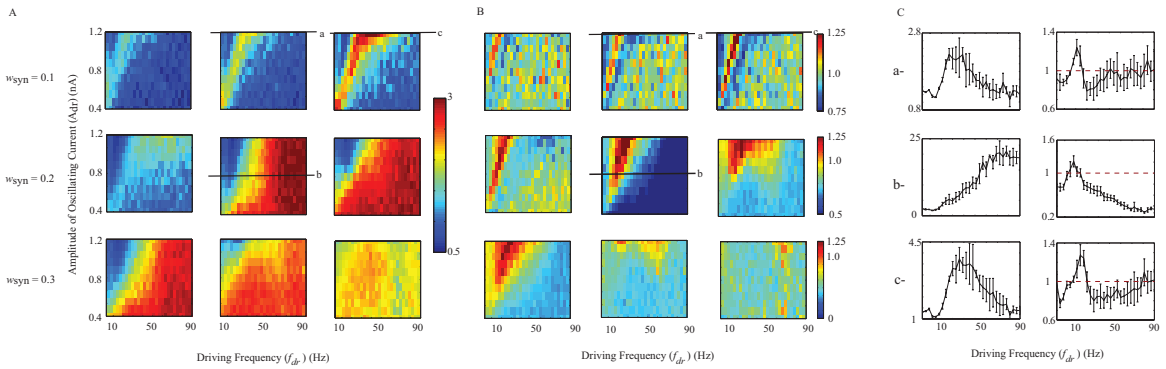

FIG. 2. Frequency dependent enhancement of the activity of the enhanced region. A) The natural log of the activity ratio for $r = 3, 4, 5$ (left, center, right respectively) and B) the MPC ratio. We vary the amplitude of the input oscillation $A_{dr} \in [0.4, 1.2]nA$ and driving frequency $f_{dr} \in [3, 90]Hz$ for three different $w_{syn} = 0.1, 0.2, 0.3$ and $r = 3, 4, 5$. C) Selected line plots for parameter values as denoted on the color figures for activity ratio (left) and MPC ratio (right) (a): $r = 4$, $w_{syn} = 0.1$, $A_{oss} = 1.2nA$; (b): $r = 4$, $w_{syn} = 0.2$, $A_{dr} = 0.8nA$ and (c): $r = 5$, $w_{syn} = 0.1$, $A_{dr} = 1.2nA$.

strength w_{syn}. Figure 1 shows vastly different spatio-temporal activity patterns depending on these parameters. At lower frequencies, for the whole range of synaptic couplings, the entire network is active due to the peaks of the slow oscillations acting as 'almost constant' depolarizing currents. At higher frequencies, and higher synaptic coupling strengths, only the enhanced region is able to maintain network driven spiking activity. This is inherently a network effect, and will be dependent on the connectivity properties (w_{syn} and r).

Overall, the network activity displayed three dynamical regimes as a function of driving frequency: a random state where the oscillation is not sufficient to stimulate the network and the activity is primarily driven by external noise; a network-wide bursting state typically mediated by slow oscillations; and a state where the enhanced region dominates the dynamics. We also observed changes in the mean phase coherence within the heterogeneity. That enhancement typically occurred for lower frequencies, just before the transition from the global bursting to increased activity of the enhanced region.

Figure 2 summarizes the network response for different parameter regimes when changing characteristics of the input current. The color plots in Figure 2A depict the natural logarithm of the activity ratio between the enhanced region and rest of the network for different values of connectivity ($r = 3, 4, 5$). Figure 2B shows the MPC ratio for the two regions. The three

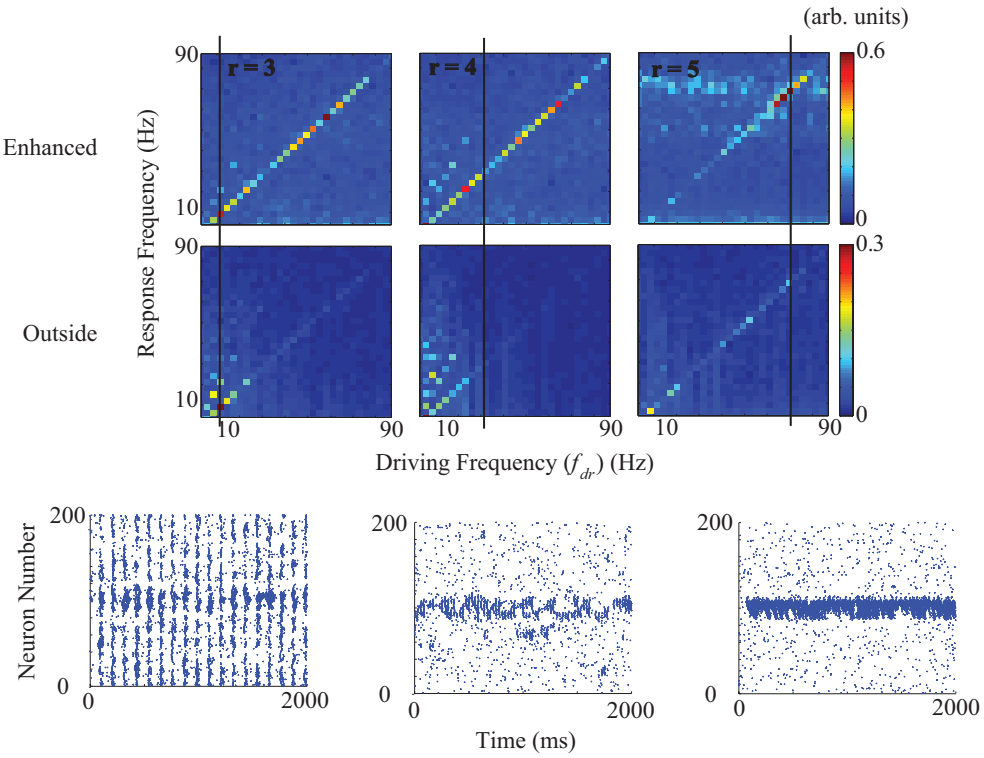

FIG. 3. Spectral Density analysis of the total network response to oscillatory drive. We plotted the PSD of the averaged activity for the enhanced (top) and outside (bottom) regions vs. the driving frequency $f_{dr} \in [3, 90]Hz$. For $r = 3, 4$, and 5 the synaptic coupling is fixed at $w_{syn} = 0.3, 0.2$, and 0.15 respectively. $A_{dr} = 0.8nA$ for all simulations. The bottom row depicts raster plots for driving frequency denoted by the black lines for $r = 3$ (left), $r = 4$ (middle), and $r = 5$ (right).

rows correspond to three different values of overall network coupling strength. The x-axis on the color plot represents the driving frequency f_{dr}, while the y-axis is the amplitude (A_{dr}).

For weak network coupling strength (Figure 2, $w_{syn} = 0.1$, all r) we observed a narrow band of increased activity ratio that is highly dependent on the driving amplitude. The changes in MPC ratio are largely insignificant, showing minimal enhancement for frequencies just preceding the activity enhancement. For the intermediate and high network coupling strength regime (for all r) we observed a significant shift of the activity increase towards the high frequency regime for all oscillatory amplitude values. Furthermore, we also observed a large frequency regime where the network heterogeneity displays an increased MPC. This occurs for low frequencies preceding the transition to enhanced region activity enhancement (Figure 2, $w_{syn} = 0.2$, $r = 4$).

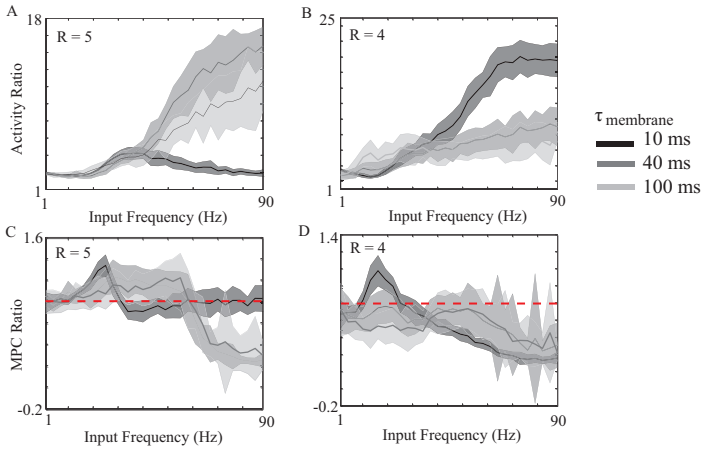

FIG. 4. Changing the membrane time constant $\tau_{membrane}$ adjusts the frequency response of the network. The activity ratio and MPC ratio for increasing membrane time constants. A and C. Oscillation amplitude is fixed at $A_{dr} = 1.2nA$, $r = 5$, and $w_{syn} = 0.1$ B and D. Oscillation amplitude is fixed at $A_{dr} = 0.8nA$, $r = 4$, and $w_{syn} = 0.1$

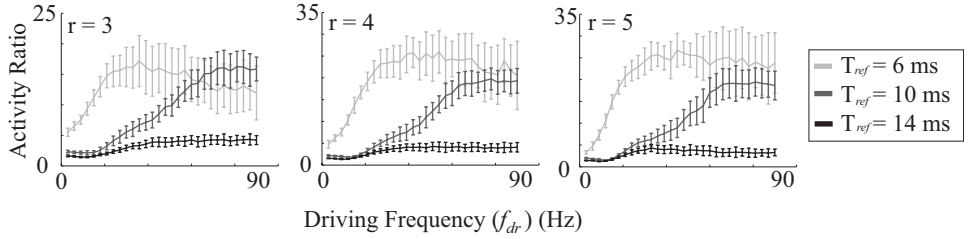

FIG. 5. Changing the refractory period (T_{ref}) adjusts the frequency response of the network. Oscillation amplitude is fixed at $A_{dr} = 0.8nA$ and $w_{syn} = 0.3, 0.2$, and 0.15 for $r = 3$, 4, and 5 respectively.

The observed changes in the activity ratios and MPCs are due to differential effects the oscillations on the two regions. In the weak coupling regime the enhanced region displays a increase of its activity for a low frequency range. This occurs because within this frequency range the cells within the enhanced region are enough depolarized to sustain network induced activity, while the neurons within rest of the network remain largely subtreshold. This effect is even more exasperated due the inhibitory layer as it further suppresses rest of the network (please refer to figure 9). For faster frequencies in the low coupling regime both network regions can not sustain the network activity and their activity ratio decreases. This frequency range is preceded by a phase locking of the neurons to a slow ($< 20Hz$) oscillatory drive

and invokes synchronous activity within the enhanced region. This synchronous activity further increases the enhanced region's ability to maintain activity because the excitatory post-synaptic potentials are highly coincident.

For the intermediate and high values of network coupling, the resonance effect is superseded by the enhanced region's propensity to easily enter a highly active, reverberatory regime with natural frequencies around 70 Hz. This reverberation is generated by the enhanced region's neurons integration time (controlled by the leakage current and synaptic input), synaptic delay, and refractory period matching the frequency of the oscillation, allowing sustained activity to quickly pass back and forth throughout the enhanced region. Basically each neuron is ready to integrate up and fire again at the peaks of each oscillation inducing a network resonance effect. Concurrently, the rest of the network is strongly inhibited by the inhibitory network receiving increased input from the enhanced region. Figure 3 also shows the network's propensity to fire at this rate (top right) and the drastically increased activity when the input frequency is in this range. Additionally Figure 3 shows how the number of connections (changing the synaptic current each neuron receives) affects the frequency dependencies. From this it is clear that increasing the number of connections decreases the integration time of the neuron, generating a stronger band of activity in the high frequency 70-80 Hz range.

A. Cellular correlates of selective activity enhancement

We investigated how the membrane characteristics affect the selective response of the enhanced region. Namely we studied the effects of the refractory period and membrane time constants on frequency dependence of the selective network activiation. Figure 4 shows the effects of varying membrane time constants has on the neuron. As we decrease the leakage, decreasing the time the neuron voltage takes to reach the threshold, the frequency at which network can sustain its activity increases. Figure 4A shows the $\sim 40Hz$ peak we achieved for our standard $\tau = 10ms$, a shift to a peak of about 70 Hz for $\tau = 40ms$, and a maximal frequency response of 80-90 Hz for $\tau = 100ms$. Accordingly the activity ratio increases because the enhanced region is firing at a higher frequency and there is increased excitation. It is also interesting to note that the MPC peaks only for the lower frequency current induced activity.

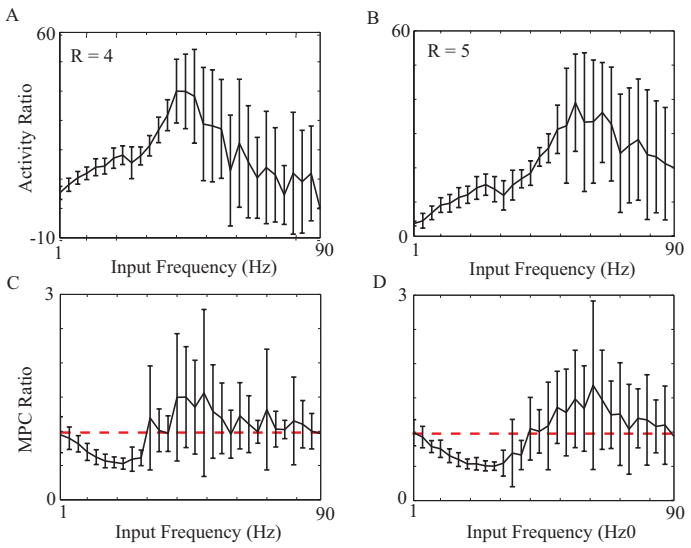

FIG. 6. Driving frequency vs. activity ratio and MPC ratio for a non resonating Hodgkin Huxley neuron. A - $r = 4$, $w_{syn} = 3$, $A_{dr} = 1.2nA$. B - $r = 35$, $w_{syn} = 2.5$, $A_{dr} = 1nA$ Simulations are averaged over 25 trials.

Figure 5 demonstrates the effect the refractory period has on the frequency dependence. Similarly to the above results, the faster refractory periods allow neurons to fire more than once under a single slow oscillation, important for sustaining activity under each peak. A 10 ms refractory period however is ideal for the high frequency regime because each neuron is simply recharging when the oscillation is in its trough. A 14 ms refractory period is too slow for either of these processes.

1. Hodgkin and Huxley neuronal network

We compared our results to a more biologically realistic Hodgkin-Huxley (HH) neuron. We used a two compartment (soma and dendrite) neuron to contrast to our integrate-and-fire results Figure 6 demonstrates the activity ratio response of these neurons to the varying input frequencies. The HH model neuron did not resonate at any frequency between 1-90Hz, but did have increased impedance at higher frequencies, indicating a weak frequency preference. It is clear that a network of HH neurons with an enhanced region allows for the same frequency-specific selective activation of the enhanced region in similar coupling and current ranges. Additionally we see a shift of the MPC to the frequency range is enhanced. This is not surprising however, because the individual neurons' frequency preference, in this

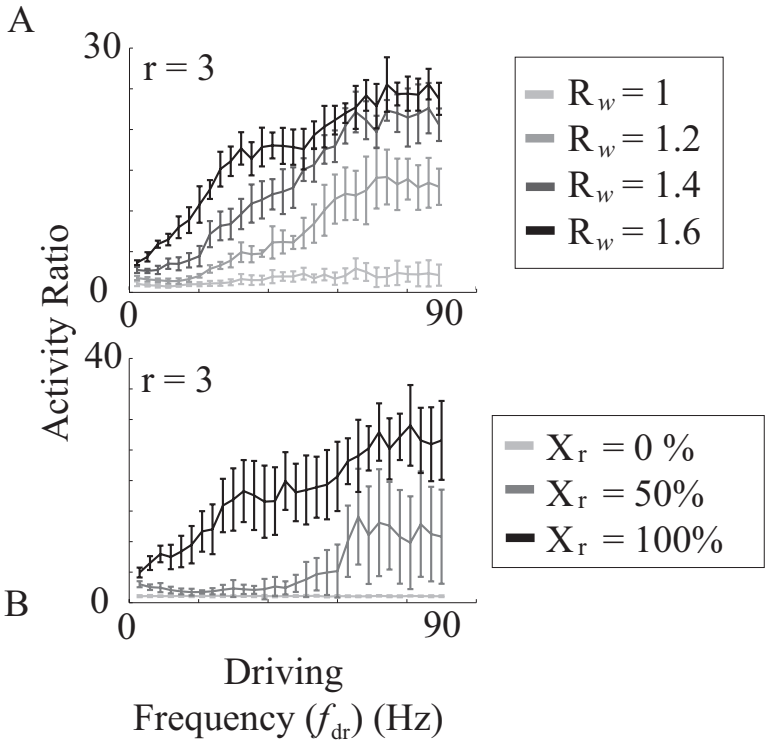

FIG. 7. Changing the connectivity in the enhanced region. A: the ratio of synaptic coupling strength (R_w) of the enhanced region vs. the rest of the network is varied. B: The enhanced region is built by randomly adding a percentage local connections within the radius $(r+2)$ for neurons in the enhanced region. For example if $X_r = 50\%$ and $r = 3$ then the neurons within the enhanced region are 100% connected from $r = 1$ through $r = 3$ and 50% connected for $r = 4$ through $r = 5$. For all simulations shown: the connectivity radius of the base network is $r = 3$, $A_{dr} = 0.8nA$ and $w_{syn} = 0.3$.

range, causes the firing rate to be modulated at this frequency, therefore enhancing the MPC. What likely occurs in the brain is a balance between these two behaviors.

While this analysis of HH neurons is by no means a thorough investigation of the possible interactions between oscillations and network in a complex neuronal model system, it proves that the observed phenomenon is network driven and independent of the specific dynamical equations of the individual cells.

B. Network correlates of selective activity enhancement

We then investigated how significant the heterogeneous enhancement needs to be to observe the robust activation differences. We did this by increasing/decreasing the synaptic coupling of the enhanced region by changing the excitatory coupling strength while keeping all other excitatory and inhibitory connections the same (Figure 7A). We observed that a relatively small increase in excitatory connection strengths within the enhanced region (around 20% over the rest of the network) allows for a significant increase in activity. This is in comparison to experimentally observed effects of spike timing dependent plasticity which can be on the order of 200%. This change in the excitatory balance provides an adaptive mechanism for the network to respond differently, depending on the overall strength of synaptic heterogeneities.

We also investigated changes in activity when we built the enhanced region through the addition of connections within the region while keeping w_{syn} the same as the rest of the network. We added connections by inserting a random fraction of additional local connections for and increased radius $(r + 2)$. Figure 7B demonstrates that a 50% increase in the number of connections was enough to increase the activity ratio. It is important to note however that this 50% increase in number of connections was significantly higher than the 20% increase in w_{syn} needed to increase the activity ratio.

1. Activity enhancement and network topology

Next we investigated how the network topology affects the enhanced region activity ratio. To do this we have varied the rewiring parameter $p \in [0, 1]$ from local $(p = 0)$ to random $(p = 1)$. We observe that as the connectivity becomes more global the activity ratio attenuates (Figure 8). This is due to the fact that as local connections are abolished the network becomes more homogeneous and random and thus the differentiation between the enhanced region ceases to exist. We still however observed significant activity enhancement for intermediate rewiring topologies near the small-world regime.

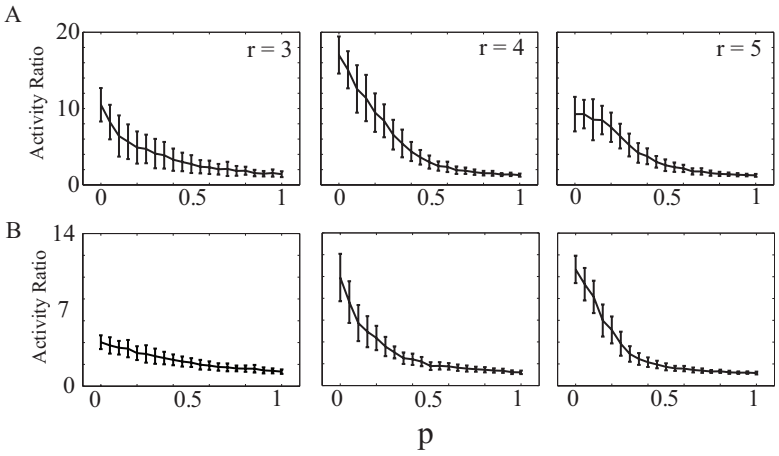

FIG. 8. Activity ratio dependence on network topology. We changed the value of the rewiring parameter p from 0 and 1 for different parameter values. Values and error bars are averaged over 50 simulations. A) $f_{dr} = 70Hz$; $A_{dr} = 0.8nA$; $w_{syn} = 0.25$; B) $f_{dr} = 30Hz$; $A_{dr} = 0.8nA$; $w_{syn} = 0.25$.

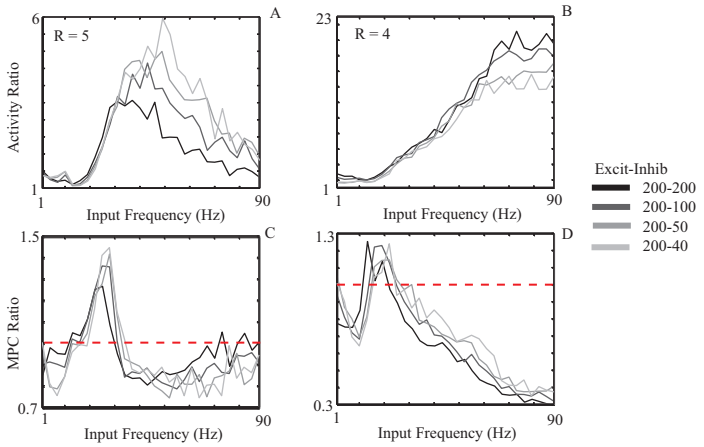

FIG. 9. Changing the ratio of excitatory to inhibitory neurons. The different ratios of excitatory to inhibitory neurons are plotted in different colors. The error bars have been eliminated for clarity. A,C) $r = 5$, $A_{dr} = 1.2nA$; $w_{syn} = 0.1$; B,D) $r = 4$ $A_{dr} = 1.2nA$; $w_{syn} = 0.2$.

2. Number of inhibitory neurons

We also investigated the effect the number of inhibitory neurons has on the network response. Figure 9 shows the activity and MPC ratio for two prevalent ranges. The other connectivity parameters of the network remain the same. Overall shape of frequency response remains the same, however there are some important changes. We observe that the

activity ratio as well as MPC ratio increase as the number of inhibitory neurons decreases, for the network parameters promoting peak at the lower frequency range. At the same time it decreases for the peak at high frequency. For high frequencies, the reduction in the peak occurs due to lowered overall inhibition generated by the enhanced region, which in turn allows the rest of the network fire at faster rate (Figure 9B).

The shift of the peak frequency and enhancement of ratio for the low frequency range is an effect of two interacting processes. The enhanced network is able to follow the oscillatory drive up to higher frequencies than the rest of the network. At the same time it generates significant amount of inhibition additionally slowing down both networks. Reduction of inhibition trough deletion of inhibitory neurons allows the non-enhanced network region to follow the oscillatory drive to higher frequencies, leading to shift of the peak frequency. At the same time it also allows the enhanced region for higher activity leading then to stronger inhibition and more thorough shutdown of other network regions 9A. Recent computational work by Fisher et al. [47] has shown that target spiking rates can be achieved in networks with different balances of excitatory and inhibitory neurons. Such a system might also respond variably to different input frequencies, as our result suggests.

This result might be especially important for the brain pathologies such as epilepsy, where it is known that seizure activity is an effect of lowered inhibition due in part to reduction of the number inhibitory interneurons. Our results indicate that this reduction could also have another dynamical effects within the heterogenous networks.

3. Frequency response of a 2-D network

All above results are based on simulations of 1-D networks, which are not biologically realistic. In this section we briefly investigated whether network dimensionality will play a significant role in the observed phenomena. We simulated a $20 * 10$ periodic 2-D network. The synaptic coupling strengths were modified to account for the increased connections for a given connection radius. Both, the actvity ratio, as well as MPC ratio show the same qualitative behaviors 10.

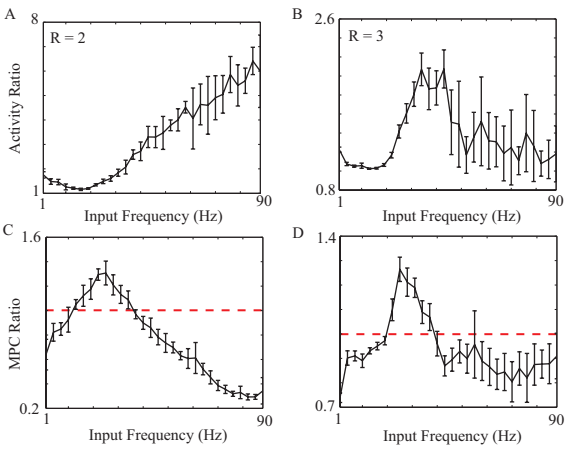

FIG. 10. Simulation for a 2-D network. A,C - $r = 2$, $A_{dr} = 1.2nA$; $w_{syn} = 0.2$. (B,D) - $r = 4$, $A_{dr} = 1.2nA$, $w_{syn} = 0.065$.

C. Cumulative cellular and network effects of a resonate-and-fire neuronal network

We have specifically chosen a non-resonating neuron model for this paper to most clearly interpret the impact of the network properties, as opposed to the resonant properties of an individual neuron. A full analysis of the interaction between a single neurons resonance and network properties will be left to another paper. In this section however, we briefly compare our results to that of a networked Izhikevich resonate-and-fire model (RAF) [44], to ensure that the responses we have observed are ubiquitous.

Here we adjusted the parameters of the RAF neuron, $w = 0.2, 0.3$, and 0.4 (all other values remain the same), to resonate at roughly 30, 45, and 60 Hz respectively. We then performed an identical analysis as previous sections with $w_{syn} = 0.3$, $A_{dr} = 1.2nA$, $r = 4$. Figure 11 shows the activity ratio and overall firing frequency of these networks RAF neurons and each frequency. We clearly see the same enhancement in the activity ratio for higher and lower frequencies (Figure 11, Column 1). The only part of the activity ratio curve that is affected is the range where single neuron resonance occurs, where the entire network is active, and the activity ratio accordingly goes to 1. We can see this range in Figure 11, Column 2.

From these results it is clear that the single neuron dynamical properties superimpose onto the network response. The network response is therefore maintained.

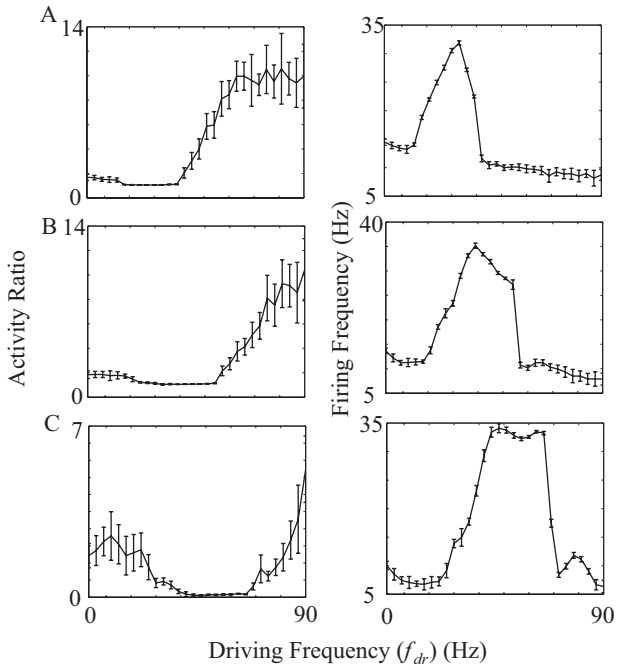

FIG. 11. Driving frequency vs. activity ratio and overall firing frequency for a RAF neuron. Row A network response for RAF neuron of resonance frequency around 30 Hz. Row B network response for RAF neuron of resonance frequency around 45 Hz. Row C network response for RAF neuron of resonance frequency around 60 Hz. The first column is the enhanced region activity ratio and the second is the overall network firing frequency.

D. Discussion and Conclusions

Oscillations are believed to have important and distinct functions in numerous regions of the brain [2, 4, 14, 28]. Their implicated roles also vary widely as a function of their amplitude and frequency [8, 48]. While high frequency gamma oscillations are thought to play an important role during focused attention and recall [2, 4], slower theta/beta band oscillations are thought to be important for learning [49, 50]. We have shown that, for a network with a heterogeneous connectivity structure, the frequency and amplitude of oscillations can play a crucial role in determining activity patterns within different network regions. While higher frequency oscillations may be optimal for the enhancements in activity of structural heterogeneities, lower frequency oscillations mediate phase locking within these heterogeneities.

These results may have also important implication for understanding pathological net-

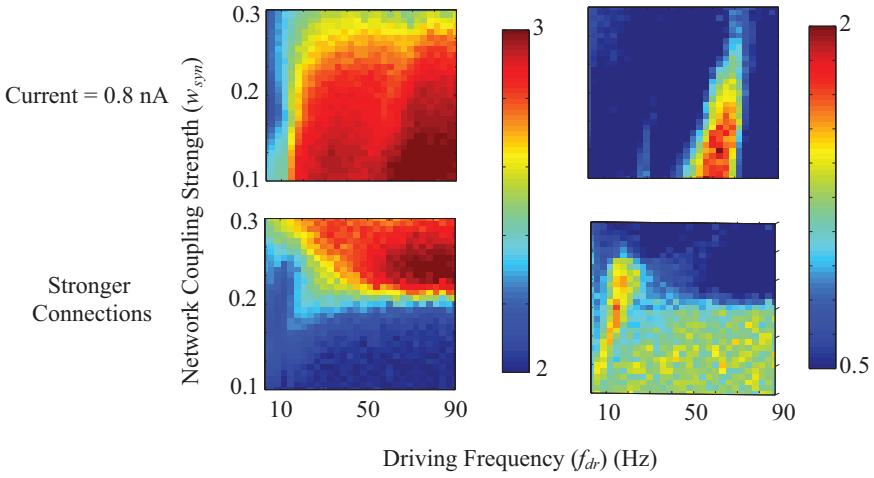

FIG. 12. Creating network heterogeneity through local depolarization. The natural log of the activity ratio (left) and the MPC ratio (right). We vary the synaptic coupling $w_{syn} \in [0.1, 0.3]$ and oscillation frequency $f_{dr} \in [0, 90]$. We investigated a depolarizing current of 0.2, for a $A_{dr} = 0.8nA$, and r = 4. We compare these results with these obtained for the structural heterogeneity.

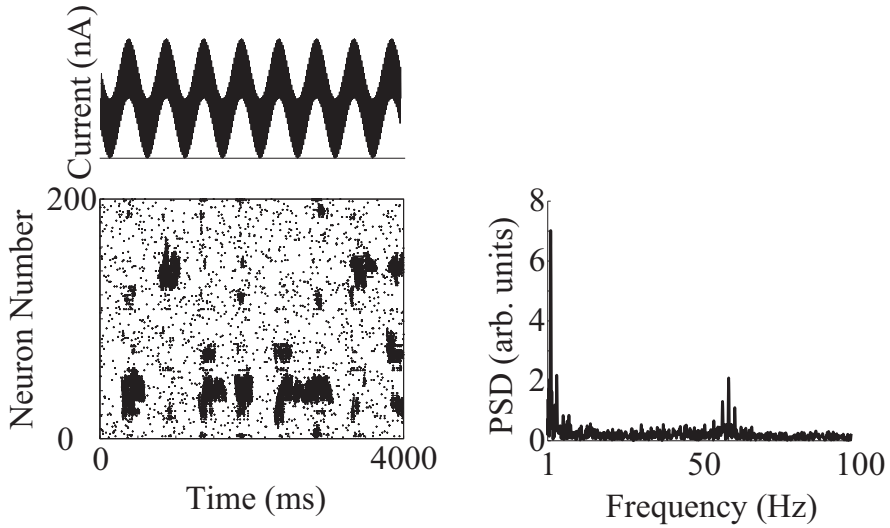

FIG. 13. A Slow + Fast Oscillatory input allows for switching between two enhanced regions. Strong 2 Hz and 60 Hz frequency component is maintained in the activity. Here $r = 5$, $w_{syn} = 0.2$ and $A_{oss} = 0.4nA$. The power spectral density shows frequency activity at low and high frequencies.

work dynamics. It has been observed that epileptic patients exhibit increased signal coherence between different brain locations in theta frequency range as compared to healthy subjects [51, 52].

Our results are due to the fact that the additional network mediated current changes, in a nonlinear fashion, the response properties of the enhanced region. These local changes to network properties can be activated by an oscillatory current within specific frequency ranges. The specific ranges depend on the neuronal refractory periods, synaptic communication times, and intrinsic current response, creating an optimal range of frequency responses.

A different response can be obtained by creating a network heterogeneity through the addition of a depolarizing current to a group of cells. Here significant enhancement is obtained throughout most the entire range of driving frequencies and the mean phase coherence increase is shifted towards higher frequencies (Figure 12), with no activity ratio peaks at specific frequencies.This suggests that a mere change of balance between excitatory and inhibitory currents due to formation of additional synapses [53] or background spikes rates [47], cannot generate the same results.

One set of processes which might employ this frequency response mechanism are those that involve higher frequency oscillations concurrent with lower frequency oscillations. A commonly observed example is gamma rhythms riding on theta rhythms during encoding and recall in the hippocampus [12]. Additionally, in recent work by Colgin et al. [2] they demonstrated that the specific frequency of a gamma oscillations was routed differentially through either the CA1 or CA3 at different phases of a theta oscillation. Another well documented use is during playback in sleep [54]. In any of these process, pre-developed short-term memory traces are reactivated for recall and/or long term encoding. This reactivation is limited to a small number of traces at a time, not global reactivation of the entire network. If we consider the enhanced region to be analogous to a short term memory trace, then the selective frequency response shown in this paper provides a mechanism allowing a input frequency to selectively reactivate that memory alone without involving other neurons and traces in the process. Figure 13 demonstrates a model system we have designed to exhibit the possible use of the interaction between fast and slow oscillations when more than one heterogeneity is present. Here we have two enhanced regions, (neuron IDs 40-60 and IDs 140-160) and we input an oscillatory current of 2 Hz and a concurrent oscillatory current of 60 Hz. At the peaks of the 2 Hz oscillation the network randomly activates one of the enhanced

regions, while the other is inhibited due to the activity from the inhibitory network. When the 2 Hz oscillation is in a trough the entire network is quiet before either of the enhanced regions are randomly activated again by the peak. Figure 13 may be representative of playback of multiple newly formed memories during REM sleep as it provides a mechanism to randomly cycle through memory traces while only activating/encoding one at a time.

In conclusion, the effects that we have discussed in this paper may provide the dynamical underpinnings to a number of brain functions that are mediated by intrinsic oscillatory patterning. For example, the increased re-activation of an already enhanced region can affect the strength of memory recall or playback during sleep [4, 26]. Additionally, increases in the coherence of neuronal activity can influence spike timing dependent plasticity between neurons, enhancing the network heterogeneity [4, 9].

This work was supported by NIH NIBIB EB008163, NSF CMMI1029388 (MZ) and Molecular Biophysics Training grant (TL T32 GM008270).

---

[1] M. D. Bevan, P. J. Magill, D. Terman, J. P. Bolam, and C. J. Wilson, Trends Neurosci **25**, 525 (2002).

[2] L. L. Colgin, T. Denninger, M. Fyhn, T. Hafting, T. Bonnevie, O. Jensen, M.-B. Moser, and E. I. Moser, Nature **462**, 353 (2009).

[3] Y. M. Akay, A. Dragomir, C. Song, J. Wu, and M. Akay, IEEE Eng Med Biol Mag **28**, 92 (2009).

[4] D. Osipova, A. Takashima, R. Oostenveld, G. Fernndez, E. Maris, and O. Jensen, J Neurosci **26**, 7523 (2006).

[5] B. Hutcheon and Y. Yarom, Trends Neurosci **23**, 216 (2000).

[6] G. Buzsaki, *Rhythms of the Brain* (Oxford University Press, New York, 2006).

[7] A. Schnitzler and J. Gross, Nat Rev Neurosci **6**, 285 (2005).

[8] S. Gielen, M. Krupa, and M. Zeitler, Biol Cybern **103**, 151 (2010).

[9] M. Shamir, O. Ghitza, S. Epstein, and N. Kopell, PLoS Comput Biol **5**, e1000370 (2009).

[10] S. M. Doesburg, J. J. Green, J. J. McDonald, and L. M. Ward, PLoS One **4**, e6142 (2009).

[11] B. Mathes, U. Pomper, P. Walla, and C. Basar-Eroglu, Neurosci Lett **478**, 14 (2010).

[12] A. Sirota, S. Montgomery, S. Fujisawa, Y. Isomura, M. Zugaro, and G. Buzski, Neuron **60**,

683 (2008).

[13] E. O. Mann and I. Mody, Nat Neurosci **13**, 205 (2010).

[14] C. S. Herrmann, I. Frnd, and D. Lenz, Neurosci Biobehav Rev **34**, 981 (2010).

[15] J. N. Brea, L. M. Kay, and N. J. Kopell, Proc Natl Acad Sci U S A **106**, 21954 (2009).

[16] P. Fries, Annu Rev Neurosci **32**, 209 (2009).

[17] M. Bartos, I. Vida, and P. Jonas, Nat Rev Neurosci **8**, 45 (2007).

[18] X. J. Wang and G. Buzski, J Neurosci **16**, 6402 (1996).

[19] M. H. Higgs and W. J. Spain, J Neurosci **29**, 1285 (2009).

[20] N. Wu, C. F. Hsiao, and S. H. Chandler, J Neurosci **21**, 3729 (2001).

[21] P. Parmananda, C. H. Mena, and G. Baier, Phys Rev E Stat Nonlin Soft Matter Phys **66**, 047202 (2002).

[22] N. W. Gouwens, H. Zeberg, K. Tsumoto, T. Tateno, K. Aihara, and H. P. C. Robinson, PLoS Comput Biol **6** (2010), 10.1371/journal.pcbi.1000951.

[23] V. S. Sohal, F. Zhang, O. Yizhar, and K. Deisseroth, Nature **459**, 698 (2009).

[24] R. Maex and E. D. Schutter, J Neurosci **23**, 10503 (2003).

[25] K. Vervaeke, A. Lorincz, P. Gleeson, M. Farinella, Z. Nusser, and R. A. Silver, Neuron **67**, 435 (2010).

[26] M. Molle, L. MArchall, S. Gais, and J. Born, The Journal of Neuroscience **22**, 10941 (2002).

[27] M. K. Sun, W. Q. Zhao, T. J. Nelson, and D. L. Alkon, J Neurophysiol **85**, 269 (2001).

[28] S. Raghavachari, M. J. Kahana, D. S. Rizzuto, J. B. Caplan, M. P. Kirschen, B. Bourgeois, J. R. Madsen, and J. E. Lisman, J Neurosci **21**, 3175 (2001).

[29] W. Singer, Cogn Neurodyn **3**, 189 (2009).

[30] Y. Wang, D. T. Chik, and Z. D. Wang, Phys Rev E Stat Phys Plasmas Fluids Relat Interdiscip Topics **61**, 740 (2000).

[31] F. Moss, L. M. Ward, and W. G. Sannita, Clinical Neurophysiology **115**, 267 (2004), 1388-2457 doi: DOI: 10.1016/j.clinph.2003.09.014.

[32] M. D. McDonnell and D. Abbott, PLoS Comput Biol **5**, e1000348 (2009).

[33] M. Perc, Physical Review E **76**, 066203 (2007), copyright (C) 2010 The American Physical Society Please report any problems to prola@aps.org PRE.

[34] Y. Yu, W. Wang, J. Wang, and F. Liu, Phys Rev E Stat Nonlin Soft Matter Phys **63**, 021907 (2001).

[35] O. Kwon and H.-T. Moon, Physics Letters A **298**, 319 (2002), 0375-9601 doi: DOI: 10.1016/S0375-9601(02)00575-3.

[36] T. Kalenscher, C. S. Lansink, J. V. Lankelma, and C. M. A. Pennartz, J Neurophysiol **103**, 1658 (2010).

[37] S. Lee, K. Sen, and N. Kopell, PLoS Comput Biol **5**, e1000602 (2009).

[38] B. Hangya, Z. Borhegyi, N. Szilgyi, T. F. Freund, and V. Varga, J Neurosci **29**, 8094 (2009).

[39] K. Morita, R. Kalra, K. Aihara, and H. P. C. Robinson, J Neurosci **28**, 1871 (2008).

[40] D. J. Watts and S. H. Strogatz, Nature **393**, 440 (1998).

[41] T. I. Netoff, R. Clewley, S. Arno, T. Keck, and J. A. White, J Neurosci **24**, 8075 (2004).

[42] H. F. Kwok, P. Jurica, A. Raffone, and C. van Leeuwen, Cogn Neurodyn **1**, 39 (2007).

[43] C. J. Stam and J. C. Reijneveld, Nonlinear Biomed Phys **1**, 3 (2007).

[44] E. M. Izhikevich, Neural Netw **14**, 883 (2001).

[45] B. Pfeuty, D. Golomb, G. Mato, and D. Hansel, Front Comput Neurosci **1**, 8 (2007).

[46] M. Florian, L. Klaus, D. Peter, and E. E. Christian, Phys. D **144**, 358 (2000), 361033.

[47] N. Fisher, S. S. Talathi, P. R. Carney, and W. L. Ditto, Biol Cybern **102**, 427 (2010).

[48] O. O. Oke, A. Magony, H. Anver, P. D. Ward, P. Jiruska, J. G. R. Jefferys, and M. Vreugdenhil, Eur J Neurosci **31**, 1435 (2010).

[49] I. Ennio, S. Antonio, C. Antonella, A. Rocco, N. Andrea, and B. Alfredo, European Journal of Neuroscience **31**, 585 (2007), 10.1111/j.1460-9568.2010.07090.x.

[50] U. Rutishauser, I. B. Ross, A. N. Mamelak, and E. M. Schuman, Nature **464**, 903 (2010).

[51] B. Clemens, Clin Neurophysiol **115**, 1436 (2004).

[52] J. Sarnthein and D. Jeanmonod, Neuroimage **39**, 1910 (2008).

[53] P. Kudela, P. J. Franaszczuk, and G. K. Bergey, Biol Cybern **88**, 276 (2003).

[54] Z. Clemens, B. Weiss, A. Szucs, L. Eross, G. Rsonyi, and P. Halsz, Neuroscience **163**, 388 (2009).